RSC Advances

ROYAL SOCIETY OF CHEMISTRY

www.rsc.org/advances

Temperature-dependent selectivity of bead-like TeO_2 nanostructured gas sensors

Sun-Woo Choi[a], and Changhyun Jin[*b]

[a]*Sensor System Research Center, Korea Institute of Science and Technology, 14-gil 5 Hwarang-ro, Seongbuk-gu, Seoul 136-791, Republic of Korea.*

[b]*School of Mechanical Engineering, Konkuk University, 120 Neungdong-ro, Gwangjin-gu, Seoul 143-701, Republic of Korea.*

* Corresponding author: *E-mail address: jinch@konkuk.ac.kr; Fax: +82 2 450 3482; Tel: +82 2 447 5886*

Abstract

Bead-like p-TeO_2 nanowires (NWs) were obtained directly from Te powder by thermal evaporation along with assisting 40 sccm of O_2 gas. Scanning and transmission electron microscopy showed that the two different formation origins for the two types of bead-like TeO_2 NWs take place at the vicinity of the surface and are characterized by (1) the presence of locally higher concentration and saturation of O_2, and (2) the surface state (terraces, ledges, and kinks (TLK)) of Te reacting with adsorbed oxygen atoms. In the present work, the gas-sensing performances of bead-like p-TeO_2 NW gas sensors fabricated using a facile and low-temperature route has been investigated for the detection of nitric dioxide (NO_2), ethanol (C_2H_5OH), and hydrogen sulfide (H_2S) gases

contained in human breath. Specifically, this work systematically investigates the gas response of bead-like p-TeO_2 NW sensors in dependence of temperature in the range from 200 °C to 400 °C. The sensing capabilities of bead-like p-TeO_2 NWs are investigated with respect to C_2H_5OH, NO_2, and H_2S without any artificial handling, such as surface modification, n- and/or p-type doping, and heterostructure formation. The selectivity of bead-like p-TeO_2 NWs by adjusting the operating temperature is dependent on the target gas, which is attributed to an interaction between p-TeO_2 NWs and gas molecules at a specific operating temperature. In particular, the bead-like p-TeO_2 NWs show quite superior sensitivity and selectivity to C_2H_5OH, NO_2, and H_2S at 250, 350, and 400 ^oC, respectively. Thus, bead-like TeO_2 NWs are promising for the detections of C_2H_5OH, NO_2, and H_2S with high selectivity at the ppm level and may contribute to the realization of more selective NW sensors.

Keywords: TeO_2; nanowires; gas sensor

Introduction

Especially, since the gas sensors require the strong chemical reaction combined with thermal stability, practical gas-sensing devices based on the large surface-to-volume ratios of 1D nanostructures are important from the viewpoint of industrial and environmental safety: (1) ensuring precise low-density limits of dangerous gases, (2) protection from carcinogenic gases, (3) protection from pollutant gases, and (4) detection of poisonous or toxic substances. Considering the merits such as high sensitivity/selectivity, quick response/recovery times, low-cost, and simplicity of fabrication, all kind of 1D nanostructures including rods, wires, belts, and tubes are ideally suited for nanoscale chemical gas sensors. In addition, the 1D nanomaterials could also enhance the sensing capability by adjusting the grain size, surface chemical properties, microstructures, addition of noble metals, as well as concentration-, thickness-, and temperature-dependent process variables. Over the past few decades, in the family of 1D nanostructured semiconducting oxides, most research for gas-sensing applications has been performed on n-type semiconductors, such as ZnO,[1] In_2O_3,[2] SnO_2,[3] TiO_2,[4] Ga_2O_3,[5] WO_3,[6] and Fe_2O_3,[7] in comparison with restricted p-type semiconductors because the mobility of negative electrons is much faster than that of positive holes to induce fast response between gas molecules and solid interactions.[8] Furthermore, for improving the gas-sensor performance, various surface modifications have been used, such as noble-metal (Pt, Pd, and Au) decoration,[9,10] controlled impurity doping,[11,12] ion implantations,[13,14] and heterostructure constructions.[15,16] Among these methods, the surface modification with protuberances is probably the easiest and most efficient route for enhancing the gas-sensor performance. Semiconducting p-type oxides, such as CuO,[17] CeO_2,[18] NiO,[19] Co_3O_4,[20] and Bi_2O_3,[21] have often been used as gas-sensor

materials for the detection of toxic/hazardous gases. Particularly, nanostructured p-type TeO_2 is one of most important semiconducting materials that has been investigated for various potential applications, such as optical storage,[22] laser devices,[23] and gas sensors.[24-27]

Meanwhile, to the best of our knowledge, there are some reports on the synthesis and sensing properties of surface-functionalized TeO_2 nanostructures in comparison to pure TeO_2 NWs.[28,29] In this regard, systematic investigations of p-type TeO_2 NWs with respect to device fabrication and sensing properties are essential for the actual implementation of p-type NWs to sensor devices.

In this study, multiple networked bead-like p-TeO_2 NW sensors were fabricated by the spray method, and their microstructure and sensing performance were examined for a wide range of operating temperatures. It has been found that the gas-selectivity of bead-like p-TeO_2 NWs is highly dependent on the operating temperature and that this material is suitable for chemical gas-sensing applications.

Experimental details

Synthesis of bead-like p-TeO_2 NWs

The bead-like p-TeO_2 NWs were fabricated on p-type Si (100) substrates after deposition of the ~3-nm thick Au catalyst. About 2 g of Te metal powder in an alumina boat along with 40 sccm of assisting O_2 gas were used in the center of a horizontal tube furnace at 400 ℃ for 1 h. The substrate was placed with 20 cm distance downstream from the centered boat containing the Te source. After carrying out the evaporation/condensation processes, the tube furnace was subsequently cooled to room temperature.

Materials characterization

The morphologies of two different types of bead-like p-TeO_2 NWs were analyzed using scanning electron microscopy (SEM, Hitachi S-4200) and transmission electron microscopy (TEM, Phillips CM-200). In addition, an energy-dispersive X-ray (EDX) spectrometer attached to the SEM was used to determine the elemental compositions of the two types of TeO_2 NWs.

Sensor fabrication and sensing measurement

The bead-like p-TeO_2 NWs were dispersed in ethanol and the colloid was coated on SiO_2/Si substrate using the spray method. Ti (~50 nm)/Pt (~200 nm) double-layer electrodes were sequentially sputtered onto the SiO_2/Si substrate coated by the randomly dispersed, multiply networked TeO_2 NWs by using an interdigital shadow mask. The sensing properties of the bead-like p-TeO_2 NWs against the gases C_2H_5OH, NO_2, and H_2S were investigated using a home-made gas-sensing system. To determine the optimal temperature for best sensing performance toward the respective gases, all sensing measurements were carried out in the range of 200–400 ^oC. It must be note that, in spite of NO_2 response at room temperature, all the sensing measurements were performed in the range of 200-400 ^oC for C_2H_5OH, H_2S, and NO_2 gases. This was due to insufficient response of p-TeO_2 NWs for C_2H_5OH and H_2S at room temperature (see ESI, Fig. S1†). The target gas concentration was regulated by mixing the air-balanced target gas and dry air using mass flow controllers (MFCs). The total flow rate was set to 500 sccm to exclude possible variation in the sensing measurements. The gas flow rate has a big influence on the sensor's gas response. Therefore, the fabricated sensors were tested the response for C_2H_5OH, NO_2, and H_2S with different gas flow rate at 250, 350,

and 400 ^{o}C, respectively. The best gas response was obtained at a 500 sccm flow rate for all gases. Based on these results, all the other sensing measurements were performed at this flow rate. The content of water vapor was negligible, according to the specifications provided by the manufacturer. The gas response R of the fabricated sensors against reducing gas was calculated by the ratio of R_g/R_a, where R_g and R_a are the resistances in the presence and absence of the target gas, respectively, For an oxidizing gas, R_a/R_g was used as gas response. The response/recovery times were defined as the times needed to reach 90% changes in resistance upon supply or removal of the target gas, respectively.

Results and discussion

Fig. 1 illustrates schematically the sensor-fabrication procedure used in this work. The first step involved is the growth of bead-like TeO_2 NWs on Si (100) substrate by thermal evaporation.[28] In the second step, the TeO_2 NWs were dispersed in ethanol and coated on a 200-nm thick SiO_2 layer formed on top of the Si substrate for fabricating the sensor platform by using an airbrush spray gun that can coat uniform thin layers on irregular-shaped substrates. In the third step, for the sensing measurements, layers of Ti (~50 nm) and Pt (~200 nm) were sequentially deposited via sputtering on the networked TeO_2 NWs using an interdigital shadow mask.

Fig. 2a–b shows SEM images of the 1D bead-like TeO_2 NWs synthesized using evaporation/condensation of Te powder with 40 sccm of assisting O_2 gas. The average diameter and length of the TeO_2 NWs were ~100 nm and a few tens of micrometers, respectively. As can be seen from Fig. 2a, the bead-like TeO_2 NWs were randomly distributed on the substrate. At first glance, TeO_2 nanoparticles are attached to all surfaces of the NWs. The existence of many protuberant nanocrystals shown in Fig. 2b

means two different possible types of nucleation formation: (1) nucleation of bead-like TeO_2 occurred readily at local regions where the O_2 concentration is higher than at other parts, (2) nucleation of bead-like TeO_2 happened quickly at saturated regions where the density of Te is enhanced via flat regions (terraces), atomic steps (ledges), and corners (kinks).[30,31] These morphologies of the bead-like TeO_2 NWs would increase the number of adsorption/desorption sites for various target gases, inducing reactions between solid and gas. The EDX spectrum presented in Fig. 2c shows that the bead-like TeO_2 NWs consist of Te and O and additional Au and Si originating from the catalyst and substrate, respectively.

Fig. 3 shows images of TEM (Fig. 3a–b), HRTEM (Fig. 3c), and the corresponding SAED pattern (Fig. 3d) of the bead-like TeO_2 NWs obtained from thermal evaporation. Figure 3a indicates even thickness at diameters below ~100 nm with uneven beads along the length direction. As mentioned above, the origin of this morphology comes from the reaction of relatively O_2-rich regions and Te at constant concentration. However, Fig. 3b shows the uniform thickness of the NW attached with a nanoparticle at protruding surface regions, such as ledges and kinks. In contrast to Fig. 3a, the source of this morphology stems from the reaction of relatively Te-rich regions at constant O_2 concentration. The local high-resolution TEM (HRTEM) image (Fig. 3c) reveals a clear fringe pattern, suggesting 0.29 nm interplanar spacing, in accordance with the (102) lattice plane of tetragonal TeO_2. The SAED pattern (Fig. 3d) supports that the bead-like TeO_2 NWs consist of single crystals, corresponding to the (010), (102), and (112) planes.

The C_2H_5OH gas-sensing properties of the bead-like p-TeO_2 NW sensors were investigated at various operating temperatures in the range of 200–400 ^oC and

concentrations ranging from 50 to 200 ppm shown in Fig. 4. As shown in Fig. 4a, all the fabricated sensors showed p-type sensing behavior. That is, the resistance increases in the presence of the reducing gas C_2H_5OH, and maintained its original value after removal of C_2H_5OH. The C_2H_5OH gas responses of the fabricated sensors at various operating temperatures are shown Fig. 4b. The best C_2H_5OH response was obtained at 250 ^oC. The response and recovery times are summarized in Fig. 4c. As evident, the response and recovery times of TeO_2 NWs to C_2H_5OH gas at 250 ^oC are of the order of some tens of seconds. Regarding the response/recovery times at different temperatures, it is sluggish in case of C_2H_5OH. Also, the C_2H_5OH response of p-TeO_2 NWs is higher than the sensors fabricated with other p-type nanostructured materials (see ESI, Table S1†).

The H_2S-sensing properties of the bead-like p-TeO_2 NW sensors have been also investigated under the same experimental conditions. The change in resistance at various operating temperatures in the range of 200–400 ^oC is displayed in Fig. 5a. It is evident that the resistances of all the fabricated sensors track the supply and stoppage of H_2S at different temperatures. It is clear that the H_2S-responses of the sensors improved with increasing operating temperature. Fig. 5b summarizes the sensor responses obtained at various temperatures. The sensors showed the best H_2S-response at 400 ^oC, the temperature that was chosen to compare the H_2S-selectivity of the bead-like TeO_2 NWs. The response and recovery times for H_2S are summarized in Fig 5c. As evident, both the response and recovery times of the bead-like p-TeO_2 NWs toward H_2S amount to hundreds of seconds.

In order to confirm the selectivity of the bead-like p-TeO_2 NW sensors toward oxidizing gases, we have tested the sensing properties of these sensors against the

representative oxidizing gas NO_2. Fig. 6a shows the dynamic response curves obtained in case of exposure to 50, 100, and 200 ppm of NO_2. The NO_2-sensing properties of the fabricated sensors are dependent on the operating temperature. Fig. 6b summarized the gas response of the p-TeO_2 NWs toward NO_2. The responses of the sensors operating at different temperatures are also included in Fig. 6b for comparison. For better description, Fig. 6c summarizes the response and recovery times of the p-TeO_2 NWs as a function of the NO_2 concentration. It is of note that the bead-like p-TeO_2 NWs showed best sensing properties with respect to gas response and response/recovery times at 350 ^oC.

For the selectivity characterization, the sensors were exposed to 200 ppm of C_2H_5OH, H_2S, CO (not shown in this work), SO_2 (not shown in this work), and NO_2 at various operating temperatures, as shown in Fig. 7. Fig. 7a shows the typical bell-shape gas response as a function of the operating temperature. The best gas response against C_2H_5OH, H_2S, and NO_2 is obtained at 250, 350, and 400 ^oC, respectively. The bell- or volcano-shaped gas-response behavior is quite common among semiconductor-based gas sensors.[32–34] In semiconducting oxide gas sensors, the response usually increases and reaches its maximum at a certain temperature, and then decreases with further increase in temperature. The competition between slow kinetics of gas molecules at low temperature and their enhanced desorption at high temperatures is likely to be responsible for this behavior. Accordingly, the use of bead-like p-TeO_2 NWs for the selective detection of gas species is rather promising. In general, pristine oxide NWs do not show enough sensing ability that they could be applied to actual sensor applications. Therefore, conventional approaches to enhancing the sensing properties of pristine NWs including decorating, doping, and surface modification were attempted.[9–12] To improve the sensing properties of p-TeO_2 NWs, similar methodologies have been carried out to

realize actual applications. In particular, one important feature of the fabricated sensors in this work is the surface modification by protuberances. Basically, the tendency in surface modification is the same as observed in case of n-SnO_2 NWs reported earlier.[35] The geometrical factors, such as NW diameter and length, and their density for best sensing performances were specifically discussed in an earlier report.[35]

Conclusions

The bead-like p-TeO_2 NWs originated from two different growth mechanisms were fabricated by evaporation/condensation of Te powder with 40 sccm of assisting O_2 gas. Many fine nanoparticles were formed at the local surfaces of the TeO_2 NWs. The existence of many rough nanocrystals helped the formation of bead-like TeO_2 nanostructures, implying suitable adsorption and desorption sites for NO_2, C_2H_5OH, and H_2S gas molecules, in turn resulting in chemical gas sensing. Especially, the optimum sensitivity of the sensors against the three investigated individual gases was clearly different and was affected only the process variable temperature without any functionalizing control, such as doping, surface modification, and heterostructures. This means that in case of the bead-like TeO_2 NWs, the optimal sensitivity and selectivity against various chemical gases could be simply adjusted by using only temperature as process variable.

Acknowledgements

This study was supported by the KU Research Professor Program of Konkuk University.

Notes and references

1. R. Khan, H. Ra, J. T. Kim, W. S. Jang, D. Sharma, Y. H. Im, *Sens. Actuators B*, 2010, **150**, 389-393.
2. W. Zheng, X. Lu, W. Wang, Z. Li, H. Zhang, Y. Wang, Z. Wang, C. Wang, *Sens. Actuators B*, 2009, **142**, 61-65.
3. Y. Shen, T. Yamazaki, Z. Liu, D. Meng, T. Kikuta, N. Nakatani, M. Saito, M. Mori, *Sens. Actuators B*, 2009, **135**, 524-529.
4. X. Cheng, Y. Xu, S. Gao, H. Zhao, L. Huo, *Sens. Actuators B*, 2011, **155**, 716-721.
5. L. Mazenia, Y. N. Picad, S. I. Maximenko, F. K. Perkins, E. R. Glaser, M. E. Twigg, J. A. Freitas, Jr., S. M. Prokes, *Cryst. Growth Des.*, 2009, **9**, 4471-4479.
6. A. Ponzoni, E. Comini, G. Sberveglieri, J. Zhou, S. Z. Deng, N. S. Xu, Y. Ding, Z. L. Wang, *Appl. Phys. Lett.*, 2006, **88**, 203101.
7. W. Jin, B. Dong, W. Chen, C. Zhao, L. Mai, Y. Dai, *Sens. Actuators B*, 2010, **145**, 211-215.
8. N. Yamazoe, G. Sakai, K. Shimanoe, *Catal. Surv. Asia*, 2003, 7, 63-75.
9. D. Kohl, *Sens. Actuators B*, 1990, **1**, 158-165.
10. T. Hsueh, S. Chang, C. Hsu, Y. Lin, I. Chen, *Appl. Phys. Lett.*, 2007, **91**, 53111.
11. N. Singh, C. Yan, P. S. Lee, *Sens. Actuators B*, 2010, **150**, 19-24.
12. K. Kim, Y. W. Song, S. Chang, I. H. Kim, S. Kim, S. Y. Lee, *Thin Solid Films*, 2009, **518**, 1190-1193.
13. K. Okamura, T. Ishiji, M. Iwaki, Y. Suzuki, K. Takahashi, *Surf. Coat. Technol.*, 2005, **201**, 8116-8119.
14. Y. Chen, C. Zhu, X. Shi, M. Cao, H. Jin, *Nanotechnology*, 2008, **19**, 205603.
15. S. Sen, P. Kanitkar, A. Sharma, K. P. Muthe, A. Rath, S.K. Deshpande, M. Kaur, R. C. Aiyer, S. K. Gupta, J. V. Yakhmi, *Sens. Actuators B*, 2010, **147**, 453-460.

16. L. Liao, Z. Zhang, B. Yan, Z. Zheng, Q. L. Bao, T. Wu, C. M. Li, Z. X. Shen, J. X. Zhang, H. Gong, J. C. Li, T. Yu, *Nanotechnology*, 2009, **20**, 085203.
17. R. L. K. Patrick, O. S. David, J. M. Benjamin, M. G. Natacha, W. W. Graeme, *J. Phys. Chem. C*, 2012, **116**, 2443-2452.
18. I. Hotovy, J. Huran, P. Siciliano, S. Capone, L. Spiecss, V. Rehacek, *Sens. Actuators B*, 2001, **78**, 126-132.
19. A. Cao, J. Hu, H. Liang, W. Song, L. Wan, X. He, X. Gao, S. Xia, *J. Phys. Chem. B*, 2006, **110**, 15858-15863.
20. X. Gou, R. Li, G. Wang, Z. Chen, D. Wexler, *Nanotechnology*, 2009, **20**, 495501.
21. S. N. B. Hodgson, L. Weng, *J. Sol-Gel Sci. Technol.*, 2000, **18**, 145-158.
22. S. N. B. Hodgson, L. Weng, *J. Mater. Sci.: Mater. Electron.*, 2006, **17**, 723-733.
23. Z. Liu, T. Yamazaki, Y. Shen, T. Kikuta, N. Nakatani, *Jpn. J. Appl. Phys.*, 2008, **47**, 771-774.
24. Z. Liu, T. Yamazaki, Y. Shen, T. Kikuta, N. Nakatani, T. Kawabata, *Appl. Phys. Lett.*, 2007, **90**, 173119.
25. T. Siciliano, A. Tepore, G. Micocci, A. Genga, M. Siciliano, E. Filippo, *Sens. Actuators B*, 2009, **138**, 207-213.
26. C. Jin, S. Park, H. Kim, C. Lee, *Bull. Korean Chem. Soc.*, 2012, **33**, 1851-1855.
27. C. Yan, B. H. Le, D. J. Kang, *J. Mater. Chem. A*, 2014, **2**, 5394-5398.
28. S. Park, S. Kim, G. Sun, W. I. Lee, K. K. Kim, C. Lee, *Nanoscale Res. Lett.*, 2014, **9**, 638.
29. Bennema P, Gilmer G H, 1973 Crystal Growth: An Introduction, ed. By P Hartman (Amsterdam: North-Holland)
30. van der Eerden J P, 1993 Handbook of Crystal Growth, vol. 1a Fundamentals

'Thermodynamics and Kinetics' (Amsterdam: North-Holland)

31. A. Kolmakov, D. O. Klenov, Y. Lilach, S. Stemmer, M. Moskovits, *Nano Lett.*, 2005, **5**, 667-673.
32. V. V. Malyshev, A. V. Pislyakov, *Sens. Actuators B*, 2008, **134**, 913-921.
33. M. Cao, Y. Wang, T. Chen, M. Antonietti, M. Niederberger, *Chem. Mater.*, 2008, **20**, 5781-5786.
34. H. W. Kim, S.-W. Choi, A. Katoch, S. S. Kim, *Sens. Actuators B*, 2013, **177**, 654-658.
35. J. Y. Park, S.-W. Choi, S. S. Kim, *J. Phys. Chem. C*, 2011, **115**, 12774-12781.

Figure captions

Fig. 1 Schematic illustration of the fabrication process of bead-like p-TeO_2 NW sensors.

Fig. 2 SEM images showing the morphologies of the bead-like TeO_2 nanowires (NWs) synthesized at 400 °C: (a) SEM image of the NWs formed at the distance of 20 cm downstream from the source powder, (b) high-magnification image of (a), (c) EDX spectrum of the bead-like TeO_2 NWs.

Fig. 3 TEM images of the bead-like TeO_2 NWs obtained by thermal evaporation: (a) TEM image originating from the region of high concentration and saturation of Te, (b) TEM image originating from the area of anisotropically distributed Te reacting with adsorped oxygen, (c) HRTEM micrograph of the bead-like TeO_2 NWs, (d) corresponding SAED pattern.

Fig. 4 (a) Change in resistance of the bead-like p-TeO_2 NW sensors for various C_2H_5OH concentrations at various operating temperature. (b) Sensor responses and (c) response and recovery times of the bead-like p-TeO_2 NW sensors.

Fig. 5 (a) Change in resistance of the bead-like p-TeO_2 NW sensors for various H_2S concentrations at various operating temperature. (b) Sensor responses and (c) response and recovery times of the bead-like p-TeO_2 NW sensors.

Fig. 6 (a) Change in resistance of bead-like p-TeO_2 NW sensors for various NO_2 concentrations at various operating temperature. (b) Sensor responses and (c) response and recovery times of bead-like p-TeO_2 NW sensors.

Fig. 7 (a) Responses to 200 ppm of C_2H_5OH, H_2S, and NO_2 as a function of operating temperature. (b) Responses to 200 ppm of C_2H_5OH, H_2S, and NO_2 at optimized temperatures.

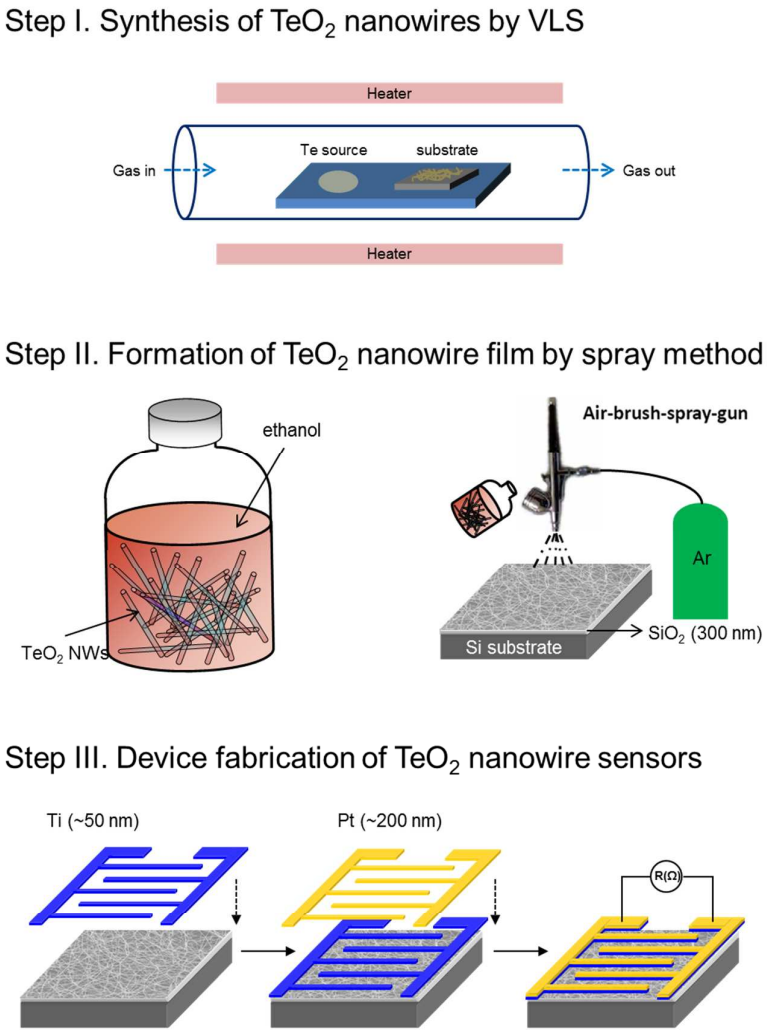

Fig. 1. Schematic illustration of the fabrication process of bead-like p-TeO_2 NW sensors.

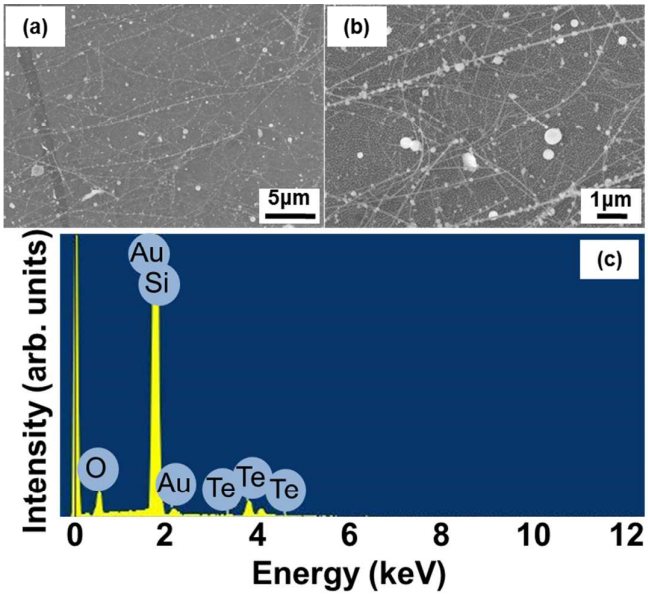

Fig. 2. SEM images showing the morphologies of the bead-like TeO_2 nanowires (NWs) synthesized at 400 °C: (a) SEM image of the NWs formed at the distance of 20 cm downstream from the source powder, (b) high-magnification image of (a), (c) EDX spectrum of the bead-like TeO_2 NWs.

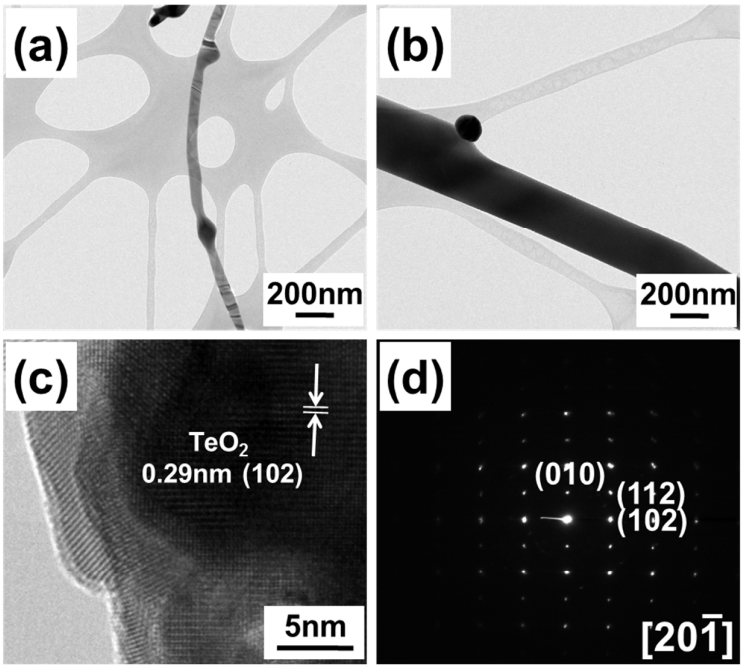

Fig. 3. TEM images of the bead-like TeO_2 NWs obtained by thermal evaporation: (a) TEM image originating from the region of high concentration and saturation of Te, (b) TEM image originating from the area of anisotropically distributed Te reacting with adsorbed oxygen, (c) HRTEM micrograph of the bead-like TeO_2 NWs, (d) corresponding SAED pattern.

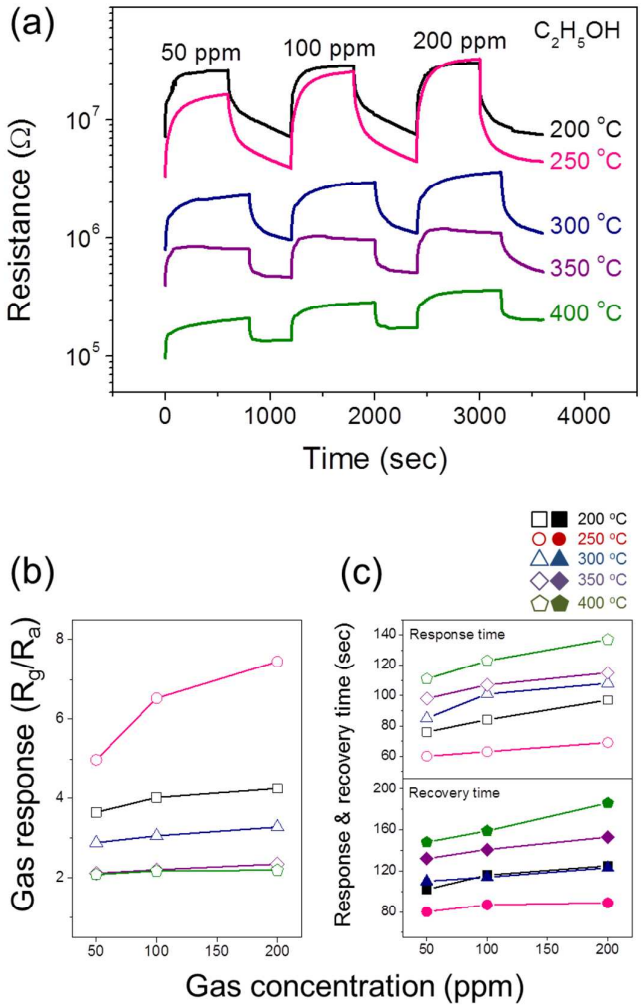

Fig. 4. (a) Change in resistance of the bead-like p-TeO_2 NW sensors for various C_2H_5OH concentrations at various operating temperature. (b) Sensor responses and (c) response and recovery times of the bead-like p-TeO_2 NW sensors.

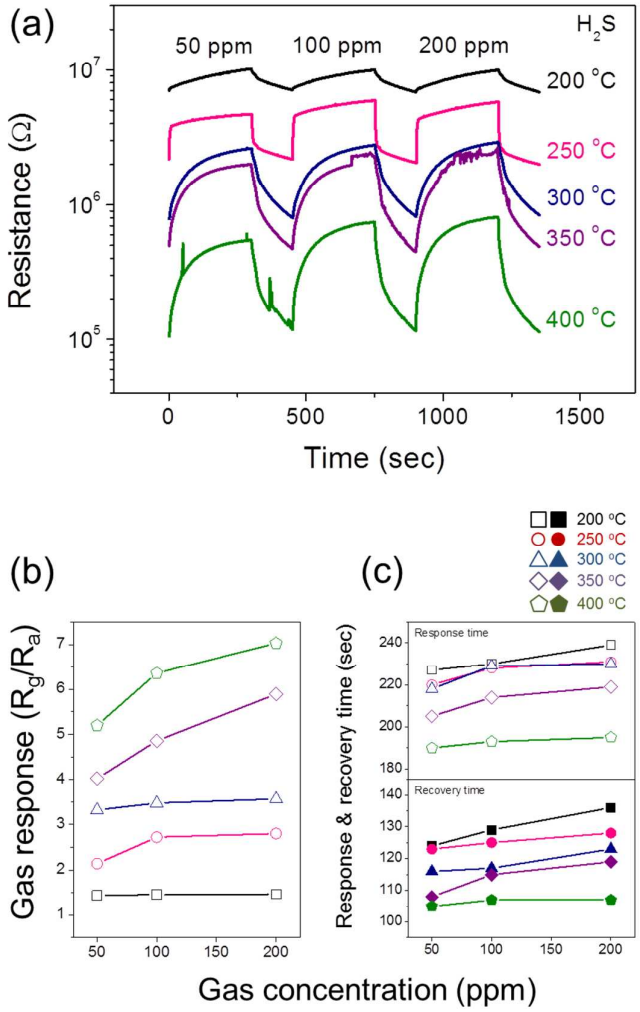

Fig. 5. (a) Change in resistance of the bead-like p-TeO_2 NW sensors for various H_2S concentrations at various operating temperature. (b) Sensor responses and (c) response and recovery times of the bead-like p-TeO_2 NW sensors.

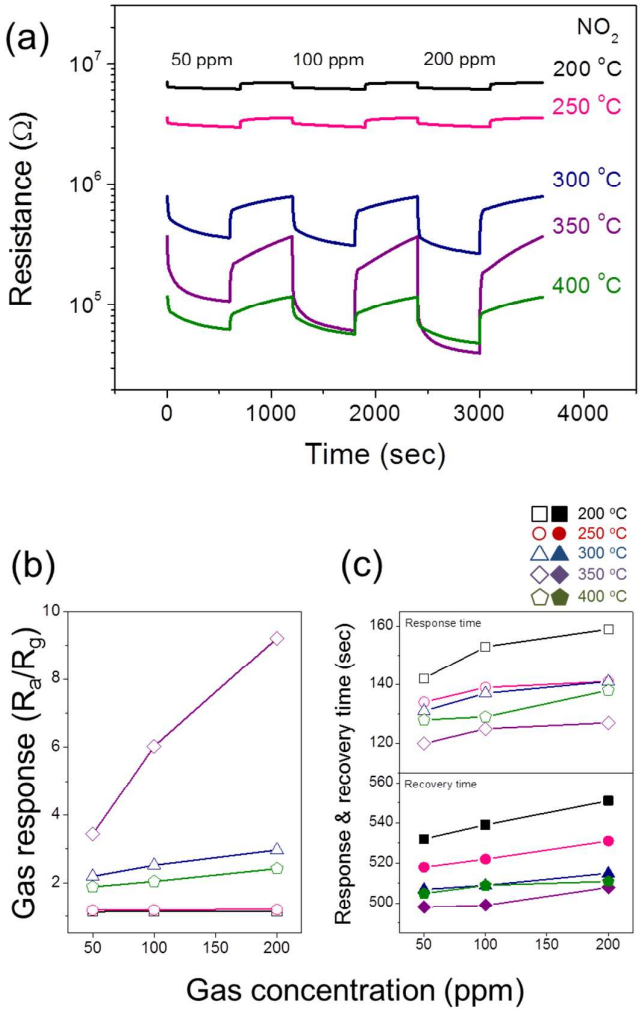

Fig. 6. (a) Change in resistance of bead-like p-TeO_2 NW sensors for various NO_2 concentrations at various operating temperature. (b) Sensor responses and (c) response and recovery times of bead-like p-TeO_2 NW sensors.

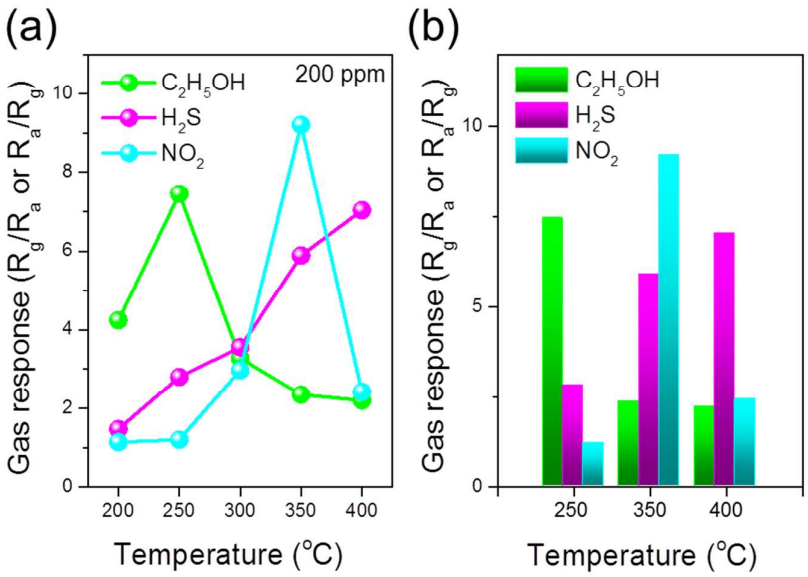

Fig. 7. (a) Responses to 200 ppm of C_2H_5OH, H_2S, and NO_2 as a function of operating temperature. (b) Responses to 200 ppm of C_2H_5OH, H_2S, and NO_2 at optimized temperatures.